

## Meson spectral functions at nonzero momentum in hot QCD\*

Gert Aarts<sup>a†</sup>, Chris Allton<sup>a</sup>, Justin Foley<sup>a</sup>, Simon Hands<sup>a</sup> and Seyong Kim<sup>b</sup>

<sup>a</sup>Department of Physics, Swansea University, Swansea, United Kingdom

<sup>b</sup>Department of Physics, Sejong University, Seoul, Korea

We present preliminary results for meson spectral functions at nonzero momentum, obtained from quenched lattice QCD simulations at finite temperature using the Maximal Entropy Method. Twisted boundary conditions are used to have access to many momenta  $p \sim T$ . For light quarks, we observe a drastic modification when heating the system from below to above  $T_c$ . In particular, for the vector spectral density we find a nonzero spectral weight at all energies.

Spectral functions provide insight into the real-time dynamics of the quark-gluon plasma. In the context of heavy-ion collisions and RHIC, lattice QCD studies carried out so far address, among others, the survival of charmonium up to  $T \sim 1.6T_c$  [ 1, 2, 3, 4], the rate of dilepton production [ 5], and transport coefficients [ 6, 7, 8, 9, 10]. Recently, analytical studies of spectral functions in strongly coupled gauge theories have also become available, using the gauge-gravity duality conjecture for  $\mathcal{N} = 4$  supersymmetric Yang-Mills theory [ 11, 12].

Meson spectral functions  $\rho_H(\omega, \mathbf{p})$  can be obtained from euclidean correlators obtained in lattice simulations by inverting the relation

$$G_H(\tau, \mathbf{p}) = \int_0^\infty \frac{d\omega}{2\pi} K(\tau, \omega) \rho_H(\omega, \mathbf{p}), \quad K(\tau, \omega) = \frac{\cosh[\omega(\tau - 1/2T)]}{\sinh(\omega/2T)}, \quad (1)$$

using the Maximal Entropy Method (MEM) [ 13]. Here  $G_H(\tau, \mathbf{x}) = \langle J_H(\tau, \mathbf{x}) J_H^\dagger(0, \mathbf{0}) \rangle$  and  $J_H(\tau, \mathbf{x}) = \bar{q}(\tau, \mathbf{x}) \Gamma_H q(\tau, \mathbf{x})$  with  $\Gamma_H = \{ \mathbf{1}, \gamma_5, \gamma_\mu, \gamma_5 \gamma_\mu \}$ . Usually only zero momentum ( $\mathbf{p} = \mathbf{0}$ ) is considered. In order to better understand the resulting spectral functions, especially at high temperature, it may be beneficial to consider spectral functions at nonzero momentum as well. There are several reasons for this [ 14]. At high temperature, spectral functions are no longer expected to be sharply peaked. Instead one expects them to have a rich structure and contain e.g. a contribution below the lightcone ( $\omega < p = |\mathbf{p}|$ ) and a momentum-dependent threshold above the lightcone. For very soft momentum and energy ( $\omega \sim p \ll T$ ) one expects hydrodynamical structure in spectral functions related to conserved currents (see refs. [ 14, 15] for more details on both continuum and lattice meson spectral functions at infinite temperature; for other recent weak-coupling

\*talk presented at Strong & Electroweak Matter (SEWM2006), BNL, United States, May 10-13 2006

†speaker, PPARC Advanced Fellow

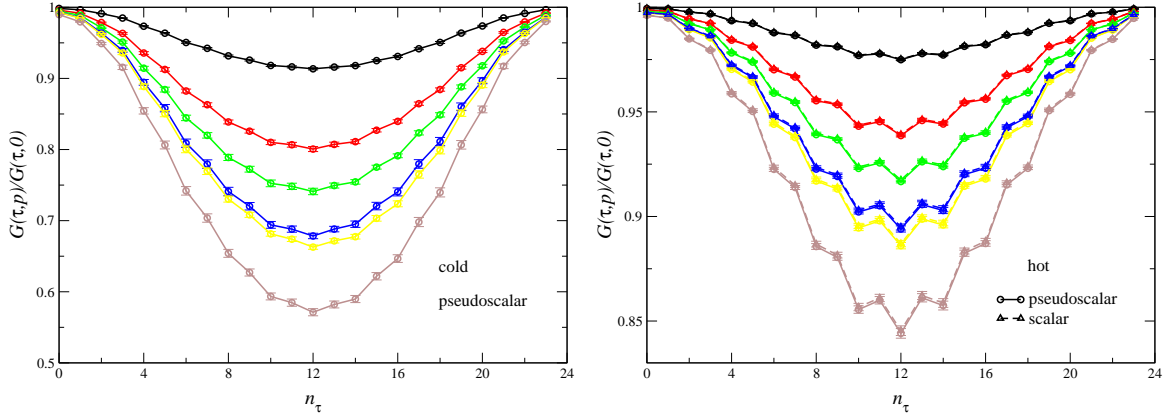


Figure 1. Euclidean correlator at nonzero momentum normalized with the correlator at zero momentum,  $G(\tau, \mathbf{p})/G(\tau, \mathbf{0})$ , in the pseudoscalar channel below  $T_c$  (left) and in the scalar and pseudoscalar channel above  $T_c$  (right). Because of chiral symmetry restoration, the latter are hardly distinguishable. The momenta are  $pL = 2.0, 3.14, 3.72, 4.25, 4.36, 5.2$  (top to bottom).

calculations, see e.g. ref. [16]). Finding specific momentum-dependent features in spectral functions obtained via MEM may help in the interpretation.

On a lattice with  $N_\sigma$  sites in a spatial and  $N_\tau$  sites in the temporal direction, the smallest nonzero momentum in units of the temperature is  $p/T = 2\pi N_\tau/N_\sigma$ . To have access to the hydrodynamic regime with many momenta  $p/T \lesssim 1$  at high temperature (with large enough  $N_\tau$  for MEM purposes) is extremely demanding. For that reason we have adopted so-called twisted boundary conditions, following closely the formulation given in ref. [17]. Combining the twisting with a standard spatial Fourier transformation, the meson momentum reads  $\mathbf{p}L = 2\pi\mathbf{n} - (\boldsymbol{\theta}_1 - \boldsymbol{\theta}_2)$ , where  $\mathbf{n}$  are integers,  $\boldsymbol{\theta}_1$  and  $\boldsymbol{\theta}_2$  are the twist angles of the two quarks, and  $L = aN_\sigma$ . In this contribution we present results on two lattices, below and above  $T_c \approx 270$  MeV, specified by

$$\begin{aligned} \text{cold: } & 48^3 \times 24, \quad \beta = 6.5, \quad a^{-1} \sim 4 \text{ GeV}, \quad T \sim 160 \text{ MeV}, \quad 100 \text{ propagators,} \\ \text{hot: } & 64^3 \times 24, \quad \beta = 7.192, \quad a^{-1} \sim 10 \text{ GeV}, \quad T \sim 420 \text{ MeV}, \quad 100 \text{ propagators.} \end{aligned}$$

The estimates for the lattice spacing and the temperature are taken from ref. [2]. Note that  $N_\tau$  is kept fixed, whereas the other parameters vary. Combining four different twist angles in a number of ways, we have  $\sim 20$  different momenta in the range  $0 < p/T < 4$  on the hot lattice. The results shown here are for light staggered quarks,  $am = 0.01$  ( $m/T = 0.24$ ).

In fig. 1 the pseudoscalar correlators both in the cold and the hot phase are presented. In order to see the relative effect of increasing the momentum we show the ratio of  $G(\tau, \mathbf{p})$  and  $G(\tau, \mathbf{0})$ . While in the cold phase the relative effect is large (up to 45% for the largest momentum shown), in the hot phase the relative effect is much less (up to 15% for the largest momentum shown). In fact, in the hot phase this effect is of the same order as the one obtained in a free quark calculation at infinite temperature (note that in the ratio the operator renormalization factors cancel). In the hot phase we also present the scalar

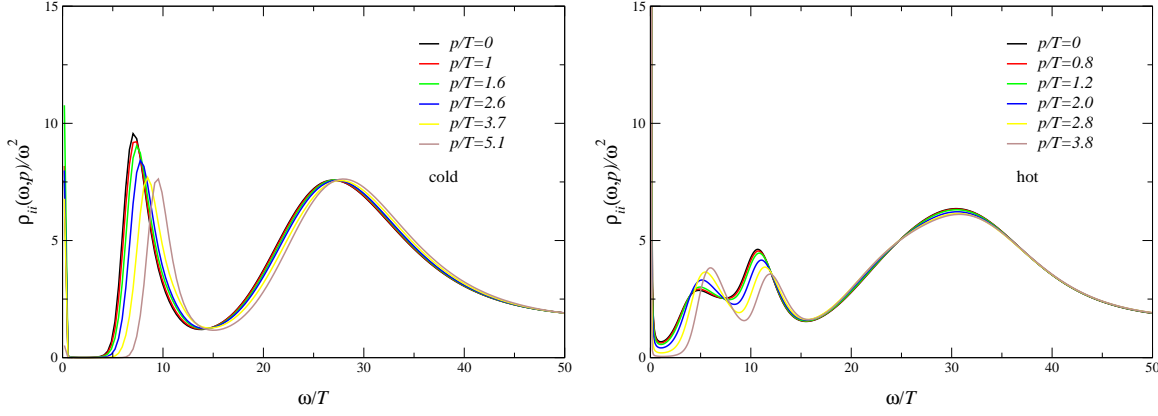


Figure 2. Spectral functions in the vector channel  $\rho_{ii}(\omega, \mathbf{p})/\omega^2$  (summed over  $i = 1, 2, 3$ ) for various values of  $p$  below  $T_c$  (left) and above  $T_c$  (right).

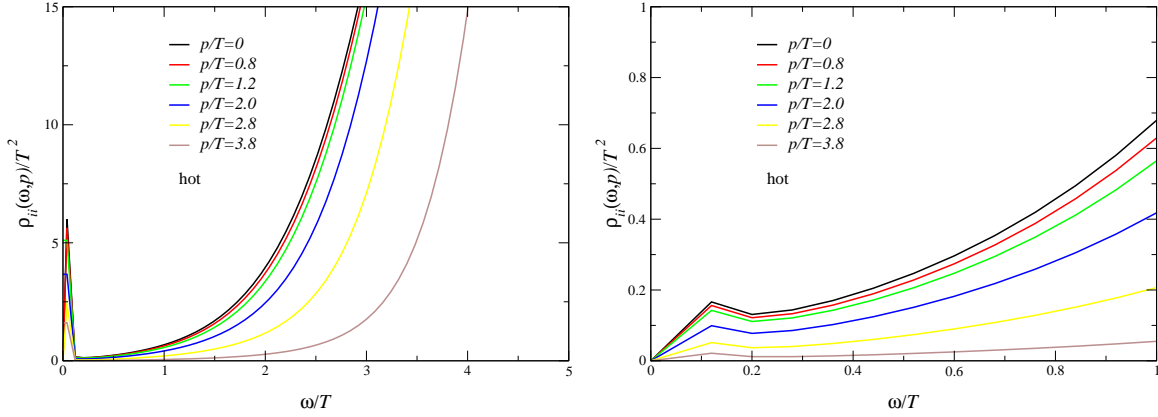


Figure 3. Left: vector spectral functions above  $T_c$ ,  $\rho_{ii}(\omega, \mathbf{p})/T^2$ , for various values of  $p$ . The sharp peak near  $\omega = 0$  is an artefact of the MEM analysis. Right: blow-up of the small-energy region with the sharp peak near zero removed.

correlator to demonstrate chiral symmetry restoration above  $T_c$ .

The MEM analysis for staggered fermions is more complicated than for Wilson fermions due to the mixing between two signals in the correlators. The equivalent of relation (1) for staggered fermions reads

$$G_H^{\text{stag}}(\tau, \mathbf{p}) = 2 \int_0^\infty \frac{d\omega}{2\pi} K(\tau, \omega) [\rho_H(\omega, \mathbf{p}) - (-1)^{\tau/a} \tilde{\rho}_H(\omega, \mathbf{p})], \quad (2)$$

where  $\tilde{\rho}_H$  is related to  $\rho_H$  by changing  $\Gamma_H$  to  $\tilde{\Gamma}_H = \gamma_4 \gamma_5 \Gamma_H$ . In practice we perform an independent MEM analysis on the even and odd time slices, obtaining  $\rho_{\text{even}} = \rho_H - \tilde{\rho}_H$  and  $\rho_{\text{odd}} = \rho_H + \tilde{\rho}_H$  and combine these to get  $\rho_H$ .

In fig. 2 we show spectral functions in the vector channel ( $\Gamma_H = \gamma_i$ , summed over  $i = 1, 2, 3$ ), normalized with  $\omega^2$ , in the cold and the hot phase. In the cold phase there is a clear bound state peak whose position shifts to larger energy with increasing momentum. The second broad structure at  $\omega/T \sim 30$  ( $a\omega \sim 1.25$ ) is probably a lattice artefact, due to

the finite Brillouin zone [ 14]. In the hot phase the bound state appears to have “melted”, although some structure remains. This requires further study. Note that the horizontal axis covers a huge range  $0 < \omega/T < 50$ . To focus on the region relevant for thermal physics, we show a blow-up of  $\rho_{ii}$ , now normalized with  $T^2$ , in fig. 3. A sudden increase is visible, which, especially for the larger momenta, appears to occur roughly when  $\omega \sim p$ . This is reminiscent of the threshold behaviour observed at weak coupling. The sharp peak at  $\omega \sim 0$  is an artefact of the MEM analysis and depends e.g. on the resolution along the  $\omega$  axis. Removing this peak by hand and zooming in even further yields the result shown in fig. 3 (right). This region is of special interest for hydrodynamics and transport, since the electrical conductivity can be defined from the slope of this spectral function at vanishing energy via the Kubo formula,  $\sigma = \lim_{\omega \rightarrow 0} \rho_{ii}(\omega, \mathbf{0})/(6\omega)$ . We note that the spectral weight is nonzero for all  $\omega$ , which is expected at high temperature. Moreover, for the smallest momenta there is a hint of a bump at small  $\omega$ . Whether this indeed corresponds to the expected hydrodynamical structure, and in particular whether the electrical conductivity can be (reliably [ 7]) extracted from the slope, requires further analysis [ 18].

## REFERENCES

1. M. Asakawa and T. Hatsuda, Phys. Rev. Lett. **92**, 012001 (2004) [hep-lat/0308034].
2. S. Datta, F. Karsch, P. Petreczky and I. Wetzorke, Phys. Rev. D **69**, 094507 (2004) [hep-lat/0312037].
3. T. Umeda, K. Nomura and H. Matsufuru, Eur. Phys. J. C **39S1**, 9 (2005) [hep-lat/0211003].
4. R. Morrin, A. P. O Cais, M. B. Oktay, M. J. Peardon, J. I. Skullerud, G. Aarts and C. R. Allton, PoS **LAT2005** (2006) 176 [hep-lat/0509115].
5. F. Karsch, E. Laermann, P. Petreczky, S. Stickan and I. Wetzorke, Phys. Lett. B **530**, 147 (2002) [hep-lat/0110208].
6. F. Karsch and H. W. Wyld, Phys. Rev. D **35** (1987) 2518.
7. G. Aarts and J. M. Martínez Resco, JHEP **0204** (2002) 053 [hep-ph/0203177].
8. S. Gupta, Phys. Lett. B **597**, 57 (2004) [hep-lat/0301006].
9. A. Nakamura and S. Sakai, Phys. Rev. Lett. **94**, 072305 (2005) [hep-lat/0406009].
10. P. Petreczky and D. Teaney, Phys. Rev. D **73** (2006) 014508 [hep-ph/0507318].
11. D. Teaney, hep-ph/0602044.
12. P. Kovtun and A. Starinets, Phys. Rev. Lett. **96** (2006) 131601 [hep-th/0602059].
13. M. Asakawa, T. Hatsuda and Y. Nakahara, Prog. Part. Nucl. Phys. **46**, 459 (2001) [hep-lat/0011040].
14. G. Aarts and J. M. Martínez Resco, Nucl. Phys. B **726** (2005) 93 [hep-lat/0507004].
15. F. Karsch, E. Laermann, P. Petreczky and S. Stickan, Phys. Rev. D **68** (2003) 014504 [hep-lat/0303017].
16. W. M. Alberico, A. Beraudo, P. Czerski and A. Molinari, hep-ph/0605060.
17. J. M. Flynn, A. Jüttner and C. T. Sachrajda [UKQCD Collaboration], Phys. Lett. B **632** (2006) 313 [hep-lat/0506016].
18. G. Aarts, C. Allton, J. Foley, S. Hands and S. Kim, in preparation.